Link sito dell'editore:
https://www.sciencedirect.com/science/article/abs/pii/S0306261915006418?via%3Dihub

Link codice DOI: https://doi.org/10.1016/j.apenergy.2015.05.031

Citazione bibliografica dell'articolo: Gianpiero Colangelo, Ernani Favale, Paola Miglietta, Arturo de Risi, Marco Milanese, Domenico Laforgia,

Experimental test of an innovative high concentration nanofluid solar collector,

Applied Energy,

Volume 154,

2015,

Pages 874-881,

ISSN 0306-2619,

*Corresponding author: gianpiero.colangelo@unisalento.it, tel. +390832297752, fax +390832297777

Experimental Test Of An Innovative High Concentration Nanofluid Solar Collector

Gianpiero COLANGELO*, Ernani FAVALE, Paola MIGLIETTA, Arturo DE RISI, Marco MILANESE, Domenico LAFORGIA

Dipartimento di Ingegneria dell'Innovazione – Università del Salento

Via per Arnesano - 73100 Lecce - Italy

Abstract

In this study, a modified flat panel solar thermal collector was built and thermal efficiency was measured with two heat transfer fluids: distillated water and Al_2O_3 – distillated water based nanofluid at high concentration (3.0%) volume fraction of solid phase. In this work for the first time nanofluid with high nanoparticle concentration has been used thanks to a modified solar thermal collector, based on patent WO2011138752 A1, which consists in bottom and top headers properly shaped in order to reduce sedimentation of clusters of nanoparticles. Thermal efficiency has been measured through an experimental setup, according to EN 12975-2 standard. Experimental results showed that an increase of thermal efficiency up to 11.7% compared to that measured with water has been obtained by using nanofluid. Besides effect of nanofluid on thermal efficiency is greater at high temperatures.

Keywords: Nanofluid, Al_2O_3, sedimentation, flat panel solar thermal collector, convective heat transfer coefficient.

Nomenclature

v_h	Inlet average velocity [m/s]
A_h	Inlet cross section area [m^2]
A_i	Cross section area at *i* position (*i=1, 2, …., 7*) [m^2]
$\dot{m}_i$	Mass flowrate at *i* position (*i=1, 2, …., 7*) [kg/s]
G	Global solar irradiance [W/m^2]
T_a	Surrounding air temperature [°C]
G_d/G	Diffuse fraction [%]
u	Surrounding air speed [m/s]
T_{in}	Collector inlet temperature [°C]

T_{out} Collector outlet temperature [°C]

$\dot{Q}$ Power extracted by solar collector [W]

c_p Specific heat [J/ kg K]

T_m Mean temperature [°C]

$\dot{m}_h$ Mass flowrate [kg/s]

A_A Absorber area of the collector [m^2]

A_a Aperture area of the collector [m^2]

T^*_m Reduced temperature difference [°Cm^2/W]

U_{Tout} Uncertainty for outlet temperature [%]

U_{Tin} Uncertainty for inlet temperature [%]

U_G Uncertainty for solar radiation [%]

U_η Uncertainty for efficiency [%]

a_1 heat transfer coefficient [W/m °C]

R^2 Uncertainty coefficient

Greek symbols

Θ Incidence angle of beam irradiance [°]

η Efficiency

η_0 Zero loss efficiency

ρ Density of the fluid [kg/m^3]

1. Introduction

The interest in improving heat transfer capability of heat transfer fluids have been growing in the last decade and particular attention has been given to nanofluids, a biphasic suspension of metal or metal oxide nanoparticles in a traditional heat transfer fluid such as water, oil, ethylene glycol [1] etc. Therefore nanofluids can also be applied in energy systems in order to increase their efficiency [2] or to enhance heat transfer coefficients in heat exchangers [3], as in cooling system for wind turbines proposed by de Risi *et al.* [4]. Thermal conductivity of nanofluids and convective heat transfer coefficient have been investigated for different materials and particle sizes by many authors [5]. Syam Sundar *et al.* [6] analyzed water and ethylene glycol mixture inseminated with Al_2O_3 nanoparticles. They obtained a thermal conductivity enhancement from 9.8% to 17.89% for Al_2O_3

nanofluid with 0.8%vol of solid phase, in a range of temperature between 15°C and 50°C. Yiamsawasd *et al.* [7] measured thermal conductivity of water based nanofluids with Al_2O_3 nanoparticles, with volume fraction from 0.0% to 8.0%, in a temperature range between 15°C and 65°C. They obtained an increase between 2% and 20%. Minsta *et al.* [8] measured thermal conductivity of water based nanofluids with Al_2O_3 nanoparticles with an average dimension of 47 nm and 37 nm respectively. An enhancement up to 30.0%, in a range of volume fraction from 1.0% to 18.0% was found. Al_2O_3-water based nanofluids at a volume fraction of 1.0%, 2.0% and 3.0% have been prepared and their thermal conductivity has been measured at 20°C by Colangelo *et al*. [9]. It was observed an enhancement up to 6.70%.

Although nanoparticles are more stable in base fluid compared with larger particles, which yield problems of clogging, abrasion and sedimentation [10 , 11], viscosity of nanofluid is higher than that of base fluid.

Convective heat transfer coefficient of nanofluids has been also investigated by many authors. Heyhat *et al.* [12] measured heat transfer coefficient of water based nanofluids with Al_2O_3 nanoparticles with an average diameter of 40.0 nm and a volume fraction from 0.1% to 2.0% in a circular tube, with constant wall temperature under turbulent flow conditions. Results were compared with convective heat transfer coefficient obtained with base fluid. An enhancement up to 23.0% was obtained. Hwang *et al.* [13] studied the convective heat transfer coefficient of water-Al_2O_3 nanofluids flowing in a stainless steel tube. The nanoparticles had an average diameter of 30 nm and they obtained an increase up to 8.0% at a concentration of solid phase of 0.3%. An increase of 20.0% and 15.0% of convective heat transfer coefficient, under laminar and turbulent flow conditions respectively, with a volume fraction of 3.0% in a stainless steel tube with an inner diameter of 4.57 mm, was obtained by Kim *et al.* [14].

Fotukian *et al.* [15] experimentally investigated that the maximum value of heat transfer coefficient enhancement is 48% for alumina nanofluids, with a volume fraction less than 0.2%, compared to water, in turbulent flow condition, inside a copper tube with inner diameter of 5.0 mm. Besides Wen *et al.* [16] found that the trend of convective heat coefficient for Al_2O_3 nanofluids (with a volume concentration from 0.6% to 1.6%) is a function of volume fraction and that in the entry region the enhancement is much higher and then it decreases with axial distance. Heris *et al.* [17] obtained enhancement of heat transfer coefficient up to 20.0% compared to that of the water with alumina nanofluids with a volume fraction from 0.2% to 2.5%. Heris *et al.* [18] observed that heat transfer coefficient of alumina nanofluids increases of 29.0%, under laminar flow condition, with a volume fraction of 2.5%. Anoop et al. [19] studied the effect of nanoparticles size on heat transfer coefficient of Al_2O_3-water based nanofluids. An enhancement of 25% for 45 nm nanoparticles and 11% for 150 nm ones at 4%wt has been obtained. Sahin *et al.* [20] determined heat transfer coefficient of Al_2O_3-water nanofluids (from 0.5%vol to 4.0%vol) in an aluminum circular tube, with inner diameter of 11.7 mm, under a constant heat flux. A parabolic trend was obtained and maximum values were measured at 1.0 %vol of solid phase.

Nanofluids can be employed in solar energy systems in order to improve their efficiency. Taylor *et al.* [21] asserted that nanofluids in a receiver of a concentrating solar thermal system can increase efficiency up to 10%. Otanicar *et al.* [22] investigated the effect of water based nanofluids on a micro scale direct absorption solar collector (DASC). Using silver nanoparticles, CNTs and graphite

nanoparticles respectively an enhancement of the efficiency with a volume fraction of 0.5% was obtained. Besides a remarkable efficiency dependence on particle size was observed for silver nanoparticles with a diameter between 20 nm and 40 nm. Yousefi *et al.* [23] investigated nanofluids effect in a flat plate solar collector using water-Al_2O_3 dispersion at a weight fraction of 0.2%. An enhancement of 28.3% in comparison with water was obtained and adding a surfactant to the suspension the efficiency enhanced of 15.63%. Chaji *et al.* [24] studied the effect of TiO_2 water based nanofluid inside a small flat plate solar collector with 0.1, 0.2 and 0.3%wt of solid phase. An index of collector total efficiency was used to compare the different cases. Efficiency was investigated at 36 l/m^{2}hr, 72 l/m^{2}hr, and 108 l/m^{2}hr respectively. An enhancement between 2.6% and 7.0% was obtained. Moghadam *et al.* [25] studied the effect of CuO – water base nanofluid at 0.4 %vol and average diameter of 40 nm on the efficiency of a flat plate solar collector. An enhancement of 4.74% and 21.8% compared to that of water has been obtained with a mass flow rate of 2 and 1 kg/min respectively.

Although nanoparticles are more stable in liquid phase than millimeter or micrometer particles, sedimentation phenomenon can be detected in piping of the systems and therefore also in solar collector, as Colangelo *et al.* [26] demonstrated with a water-Al_2O_3 nanofluid with a volume fraction between 1.0% and 3.0%. They proposed a modified flat plate solar collector to avoid this phenomenon, in order to maintain a constant flow velocity along both bottom and top header. The sedimentation analysis was carried out through an optical investigation. For this purpose, a modified flat plate solar collector was built with transparent tubes.

The aim of this work is to continue the research on a modified flat plate solar collector analyzed by Colangelo *et al.* [26] and to evaluate the increase of performance of a flat plate solar collector due to the use of water-Al_2O_3 nanofluid as heat transfer fluid. In particular, a modified flat plate solar collector using water-Al_2O_3 nanofluids was built and its efficiency was measured under different working conditions, according to EN 12975-2 standard. In this work for the first time the performance of a nanofluid solar collector is evaluated according to EN 12975-2 standard [27]. In other works the experimental campaign has been carried out using a traditional solar collector with no compliance to any standard. In this work, instead, a new model of solar collector has been designed and built, able to work specifically with nanofluids and all the experimental tests have been carried out following the EN 12975-2 standard. In this way the comparison between the heat transfer fluids has been performed in controlled and standard conditions, reducing the possibility of error. In this work a volume fraction of 3.0% of nanoparticles has been chosen to evaluate the possible problems related to sedimentation and to collect data about the most stressing conditions for the system. Other works used lower nanoparticle concentrations [22 , 23 , 24 , 25] to avoid inevitable sedimentation problems and to reduce pumping problems. In this work, for the first time, it was possible to obtain experimental data using high nanoparticles concentration, due to the peculiar design of the header tubes of the new solar collector, studied on purpose, that is able to avoid sedimentation problems, that are present in traditional solar collectors and that make impossible to carry out such experiments with high nanoparticle concentration.

2. Nanofluid preparation

Commercial Al_2O_3 nanoparticles and distillated water were used to prepare nanofluid with a volume fraction of 3.0% of nanoparticles, which have spherical shape, density of 3700 kg/m^3 and average diameter of 45 nm. No dispersant was used. The suspension was mixed with a magnetic stirrer at 700 rpm for 60 minutes and vibrated in an ultrasonic bath at 59 kHz and 285 W for 180 minutes to break the nanoparticles cluster to improve stability. Finally a second mixing with magnetic stirrer was made.

Al_2O_3 nanoparticles have been chosen because they are more stable in water and cheaper than other materials. Therefore they are a good compromise considering stability, costs and thermo-physical properties of nanofluids [26]. Stability of nanofluid was investigated with Turbiscan LabExpert. It consists in a detection head that moves along a cylindrical cell, where the nanofluid sample is placed. The detection head has a near infrared light source (λ= 800 nm) and two detectors that receive the light transmitted through the sample and the backscattered light respectively. The backscattering variation value is directly proportional to the variation of particles concentration at every position along the cell. Stability of the suspension was measured for 2 h at 25°C and Figure 1 shows backscattering during measurement. Only at the bottom of the cell a delta backscattering of 7.5% was measured, while in other positions this variation is negligible. This means that a little part of solid phase is sedimented (very large cluster nanoparticles that ultrasonic bath was not able to reduce), while the remaining solid phase is stable in the suspension.

Figure 1 – Delta backscattering measurement of Al_2O_3 water based nanofluid at 3 %vol

Average cluster size of the solid phase of nanofluid was measured using DLS technique (Zetasizer Nano – S – Malvern Instruments). Three measurements have been made and the mean value was calculated. An average diameter of 128.2 nm has been obtained, as shown in Figure 2.

Figure 2 – Cluster dimension of Al_2O_3 water based nanofluid at 3 %vol

Thermal conductivity of water and water – Al_2O_3 3.0 %vol nanofluid was measured through hot-wire technique, according to ASTM D 2717-95 standard. Water thermal conductivity was 0.606±0.006 W/m °C and an enhancement of 6.5 % was obtained with nanofluid (0.645±0.006 W/m °C) at 20°C.

3. Flat panel solar thermal collector

An innovative flat panel solar thermal collector, working with nanofluid, was designed and built. For both top and bottom header, copper tubes with inner diameter of 20.0 mm and thickness of 1.0 mm respectively were used, while copper tubes with inner diameter of 10.0 mm and thickness of 1.0 mm respectively were employed for riser tubes. The tubes were fixed on a 1332x860 mm copper plate

through thermal adhesive. Tubes and copper plate, called absorber, were coated with a black paint (Figure 3).

Figure 3– Tubes and copper plate fixed and coated with black paint (Absorber)

The absorber was inserted inside a galvanized steel frame, covered with a polycarbonate plate and insulated with a glass wool mattress and polyurethane panel (Figure 4).

A copper wedge shaped element was inserted inside the top and bottom header to maintain a constant flow velocity in order to avoid sedimentation phenomenon. In fact, as Figure 5 shows, in a traditional flat panel solar thermal collector, inside the bottom header flow rate decreases because the fluid is distributed to the riser tubes. Similarly, inside top header flow rate increases because heat transfer fluid comes out from the riser tubes.

Figure 4– Flat panel solar thermal collector

Figure 5– Flow in a traditional flat panel solar thermal collector

These variations of velocity yield sedimentation phenomenon of solid phase along both top and bottom header. In particular the amount of precipitated material is inversely proportional to the mean velocity on the cross section, as explained in [26]. Therefore through a shaped element it is possible to vary the cross section along longitudinal axis in order to maintain a constant velocity. Referring to Figure 5, $\dot{m}_h$ is the mass flow rate at the inlet of the bottom header:

$$\dot{m_h} = \rho v_h A_h \quad (1)$$

where ρ [kg/m^3] is the density of the heat transfer fluid, v_h [m/s] is the average velocity at the inlet cross section and A_h [m^2] is the cross section area. For each cross section, in order to maintain a constant velocity, it is possible to write mass flow rate as:

$$\dot{m}_i = \rho v_h A_i \ (i = 1,2, \dots ,7) \quad (2)$$

therefore

$$A_i = \frac{\dot{m}_i}{\rho v_h} \ (i = 1,2, \dots ,7) \quad (3)$$

Flat panel solar thermal collector used in this investigation has eight riser tubes. Considering an uniform distribution of the fluid to all riser tubes, $\dot{m}_i$ can be calculated through the following equation:

$$\dot{m}_i = \dot{m}_h \left(1 - \frac{i}{8}\right) \ (i = 1,2, \dots ,7) \quad (4)$$

Substituting equations (1) and (4) in equation (2), A_i can be written as:

$$A_i = A_h\left(1 - \frac{i}{8}\right) \quad (i = 1,2,\dots,7) \tag{5}$$

A generic cross section, A_i, along bottom header is a circular segment of area:

$$A_i = \frac{r^2}{2}\left(\frac{\alpha_i \pi}{180} - \sin\alpha_i\right) = A_h\left(1 - \frac{i}{8}\right) \quad (i = 1,2,\dots,7) \tag{6}$$

where α_i is the central angle in degrees and r is the inner radius. It is possible to obtain α_i from equation (6), for example A_7=3.925·10^{-5} m^2 and $\alpha_7 \approx 101°$. Shaped element inserted in both top and bottom header guarantees that in each cross section area is less than or equal to A_i.

Besides, in every cross section, velocity has a vertical component from the bottom to the top that yields a mixing between liquid and solid phase that enhances mixing of the suspension (Patent WO2011138752 A1).

Figure 6 shows the top header (or bottom header) with the shaped element.

Figure 6– Top header (or bottom header) with modified internal shaped element

4. Experimental setup

The experimental setup to measure efficiency of flat panel solar thermal collector was based on EN 12975-2 standard and is schematically shown in Figure 7. The experimental tests of the solar collector were carried out at University of Salento in Lecce, Italy (latitude is 40°20'04.5" N and longitude is 18°06'47.5" E). In a closed hydraulic circuit with expansion tank (9), heat transfer fluid flows by means of a pump (13). The system has a solenoid valve (11) on a bypass to adjust flow rate of heat transfer fluid and a safety valve (8) to protect the system from overpressure. Flow rate is measured by a Coriolis flow meter, Micro Motion® series F025S (5). If possible, efficiency measurements shall be made over a temperature range between ambient temperature and 80°C, under clear sky conditions [27]. For this purpose inlet temperature of solar collector is adjusted by band heaters (12) controlled by a PID circuit. Thermal equilibrium is guaranteed by a shell and tube heat exchanger (14) and an air-water heat exchanger (15). 4-Wire Pt100 sensors (6) are used to measure both inlet and outlet temperature of solar collector and heat exchanger. Pt100 were arranged at no more than 200 mm from both the collector inlet and outlet. Another Pt100 (6a) is used by PID circuit of band heaters. The system has two pyranometers (LP PYRA 02, Delta Ohm srl). The first one (2) measures direct irradiance on solar collector. The second one (3) is employed to measure diffuse irradiance. An anemometer (4) and a thermometer (17) measure wind velocity and air temperature respectively. Finally a radial ventilator is placed to guarantee a constant air speed over the collector (16).

Figure 7-Layout of experimental setup

Figure 8– a) Experimental setup and b) flat panel solar thermal collector

A steady-state method is used to calculate solar collector's efficiency, according to EN 12975-2 standard. The test conditions are shown in Table 1 [27 28].

Table 1 – Test conditions and deviation

The power extracted by solar collector, $\dot{Q}$, is calculated with equation (7):

$$\dot{Q} = \dot{m}_h c_p (T_{out} - T_{in}) \quad (7)$$

where c_p is the specific heat of the fluid at mean temperature, calculated with equation (8):

$$T_m = \frac{T_{out}+T_{in}}{2} \quad (8)$$

and $\dot{m}_h$ is the mass flowrate. $\dot{Q}$ can also be obtained through efficiency, η (equation (9)):

$$\dot{Q} = AG\eta \quad (9)$$

where A can be referred to the absorber area (A_A) or to the aperture area of the collector (A_a).

The instantaneous efficiency is calculated by statistical curve fitting, using the least squares method as in equation (10) [27]:

$$\eta = \eta_0 - a_1 T_m^* - a_2 G (T_m^*)^2 \quad (10)$$

where η_0 is the zero loss efficiency and T_m^* is the reduced temperature difference as defined in equation (11):

$$T_m^* = \frac{T_m - T_a}{G} \quad (11)$$

In equation (10) a second order fit shall not be used if the value of a_2 is negative. In these conditions efficiency can be calculated with equation (12):

$$\eta = \eta_0 - a_1 T_m^* = \eta_0 - a_1 \left(\frac{T_m - T_a}{G}\right) \quad (12)$$

η is calculated through equation (9) and equation (10) as described in equation (13):

$$\eta = \frac{\dot{Q}}{AG} = \frac{\dot{m}_h c_p (T_{out} - T_{in})}{AG} \quad (13)$$

Therefore η depends on $\dot{m}$, T_{out}, T_{in} and G. Mass flow rate was measured with an uncertainty $U_{\dot{m}}$<1.0%. Uncertainties for outlet and inlet temperatures, $U_{T_{out}}$ and $U_{T_{in}}$, were less than 0.1 °C. Finally solar radiation was measured with an uncertainty U_G<2.0%. Table 2 summarizes these uncertainties.

Table 2 – Measurement uncertainties

Complex uncertainty, U_η, was calculated with equation (14) and was between 0.90% and 5.76%.

$$U_\eta = \sqrt{\left(\frac{\partial \eta}{\partial \dot{m}_h} U_{\dot{m}}\right)^2 + \left(\frac{\partial \eta}{\partial G} U_G\right)^2 + \left(\frac{\partial \eta}{\partial T_{out}} U_{T_{out}}\right)^2 + \left(\frac{\partial \eta}{\partial T_{out}} U_{T_{in}}\right)^2} \quad (14)$$

5. Results and discussion

Efficiency of thermal solar collector was investigated with distillated water-Al_2O_3 nanofluid at a concentration of 0% and 3.0%vol. This volume fraction of solid phase was chosen on the basis of the experimental investigation carried out by Colangelo *et al.* [26], regarding heat transfer coefficient of alumina water based nanofluid, prepared with the same materials used in this work.

The values of mass flowrate were close to those used to investigate sedimentation of nanofluid inside solar collector with transparent tubes [26]. Flow rate variation was less than 10.0% from one test period to another one, as required by EN 12975-2 standard.

Thermal efficiency analysis of solar collector, with water and nanofluid, was carried out by testing at various reduced temperature difference, T_m^*, and in several months of the year, as shown in Table 3 and Table 4.

Testing procedure consists in measuring parameters needed to calculate efficiency of thermal solar collector at a fixed inlet temperature, which is controlled by the PID circuit. A pre-conditioning period, larger than 15 minutes, is necessary before measurement period starts. Measurement time must be not less than 10 minutes, as required by EN 12975-2 standard. Table 3 and Table 4 show experimental results for both distillated water and Al_2O_3 – distillated water nanofluid 3.0 %vol. With distillated water, the highest efficiency value, 0.4921, has been obtained with a T_m^* of 0.00958 °C m^2/W, which corresponds to an inlet temperature of 30.62 °C, an ambient temperature of 24.34 °C and a solar irradiance of 987.63 W/m^2. Instead at T_m^* of 0.04121 °C m^2/W the lowest efficiency value has been obtained, 0.3285. In this case inlet temperature, ambient temperature and solar irradiance were 66.35 °C, 33.59 °C and 840.78 W/m^2 respectively.

By using nanofluid as heat transfer fluid the highest efficiency value, 0.5412, has been obtained at inlet temperature of 37.09 °C, ambient temperature of 33.37 °C and solar irradiance of 849.06 W/m^2. At these conditions T_m^* is 0.00804. The lowest efficiency, 0.4570, was obtained at T_m^*=0.04099 °C m^2/W for inlet temperature of 64.31 °C, ambient temperature of 32.60 °C and solar irradiance of 839.88 W/m^2.

Table 3– Experimental results for bi-distillated water

Table 4– Experimental results for Al_2O_3 – bi-distillated water nanofluid 3.0 %vol

Therefore, the better results have been obtained using Al_2O_3 – water nanofluid, in the investigated reduced temperature difference range. Nanoparticles yield an enhancement of themophysical properties due to interactions between liquid and solid phases. For example one of these can be the ballistic phonon transport when particles distance is very small [29]. This phenomenon is inversely proportional to the particle size, where the ballistic phonons initiates and persists in the liquid reaching another particle, because the phonon free path is shorter in the liquid than in the solid. This happens if the separation between particles is comparable with liquid layer around the particle. For other authors Brownian motion enhances heat transfer inside suspensions due to collision between liquid molecules and solid particles [30]. Also in this case effect of Brownian motion is inversely proportional to the particle size. These heat transfer mechanisms determine an increase of thermal conductivity of nanofluid compared to that of liquid phase. By using nanofluids convective heat transfer coefficient enhancement is also obtained and it is greater than that of thermal conductivity. For example with Al_2O_3 nanoparticles at 3 %vol thermal conductivity increases of 6.7% compared to bidistilled water only. At the same volume fraction, heat transfer coefficient of Al_2O_3 nanofluids is increased up to 25% [26]. For all these reasons thermal efficiency of solar collector increases by using nanofluids. In fact, random movement of solid phase flattens temperature distribution on cross section of the tubes and increases temperature gradient between fluid and inner surface of the riser tubes. Therefore an enhancement of heat transfer is obtained [26 , 31]. A comparison on the graph is shown in Figure 9. It is possible to note that for values of T_m^* around 0.0088 °C m^2/W, efficiency of solar collector with water is between 0.4747 and 0.4912, while with nanofluid it is between 0.5153 and 0.5412. Therefore, the average efficiency measured in this range of T_m^* is 0.4826 and 0.5299 for water and nanofluid respectively. The difference between these average efficiencies is about 4.7%. Similarly, around 0.01579 °C m^2/W the average efficiency measured is 0.4460 for water and 0.5137 for nanofluid, with a difference of 6.8%. A difference of average efficiencies of 11.7% has been obtained around 0.02487 °C m^2/W, as well as at 0.03962 °C m^2/W. In fact, observing the trend lines of experimental results, it is possible to note that not only the thermal efficiency of solar collector with nanofluid is higher than that with distillated water for each reduced temperature difference, but the trend line obtained with nanofluid has a slope lower than water only.

Figure 9– Thermal efficiency of solar collector with water (mass flow rate 0.02±0.0008 kg/s) and Al_2O_3 – bi-distillated water 3.0 %vol (mass flow rate 0.02±0.0015 kg/s)

Table 5 indicates η_0, a_1 and R^2 values for instantaneous efficiency according to the equation (12). An increase of about 7.0% of the zero loss collector efficiency, η_0 (η at T^*_m=0), has been obtained by using nanofluid (from 0.517, for water, to 0.553 for nanofluid), as well as a_1 changes from 4.452 W/m °C to 2.053 W/m °C.

Table 5 - Values of the zero loss collector efficiency η_0, the heat transfer coefficient a_1 and the uncertainty coefficient R^2

Therefore, the following experimental equations of efficiency of thermal solar collector for water and nanofluid are obtained:

$$\eta_{water} = 0.517 - 4.452T_m^* \quad (15)$$

and

$$\eta_{nf} = 0.553 - 2.053T_m^* \quad (16)$$

Conclusions

A modified flat panel solar thermal collector, to avoid sedimentation of solid phase, was built and an experimental comparison of thermal efficiency between two heat transfer fluids (Al_2O_3 – distilled water based nanofluid, at 3% in volume fraction, and distilled water), working in the same thermal solar collector, has been performed. Due to its capability of drastically reducing nanofluid sedimentation inside the tubes, this solar collector made possible, for the first time, to carry out experiments with high nanoparticle concentration.

The modification of the new solar collector consists in a wedge shaped element inserted in both top header and bottom header in order to maintain a constant velocity along longitudinal axial, because amount of precipitated material, in a cross section, is inversely proportional to mean velocity. Efficiency was calculated at various reduced temperature difference, T_m^*, to which correspond different solar irradiance and inlet temperature in the solar collector. In particular, with distillated water, thermal efficiency was between 0.4921 and 0.3285 for T_m^* between 0.00855 and 0.04121. By using Al_2O_3 – water based nanofluid, thermal efficiency of solar collector was between 0.5412 and 0.4570 for T_m^* between 0.00804 and 0.04099. Therefore, nanofluid increases efficiency of flat panel solar thermal collector. Besides, from the experimental results, it has been observed that the zero loss collector efficiency η_0 of solar thermal collector with Al_2O_3 – distilled water based nanofluid is 7% higher than that with distilled water. Finally, the slope of trend line of efficiency with nanofluid is lower than that with water. Therefore, nanofluid is more effective at high temperature.

Acknowledgements

This work was supported by the SOLAR project (DM19447), funded by the Italian Ministry of University and Research (MIUR).

References

1 Xuan Y, Li Q, Heat transfer enhancement of nanofluids, Int J Heat Transfer Fluid Flow 2000; 21: 58-64;

2 Mahian O., Kianifar A., Kalogirou S.A., Pop I., Wongwises S., A review of the applications of nanofluids in solar energy, Int. J. Heat Mass Trans. 57 (2013) 582-594.

3 Kulkarni Devatta P, Das Debendra K, Vajjha Ravikanth S, Application of nanofluids in heating buildings and reducing pollution, Appl Energy 2009;86:2566–2573;

4 de Risi A , Milanese M, Colangelo G, Laforgia D, High efficiency nanofluid cooling system for wind turbines, Thermal Science 2014;18(2):543-554;

5 Lomascolo M, Colangelo G, Milanese M, de Risi A, Review of heat transfer in nanofluids: Conductive, convective and radiative experimental results, Renewable and Sustainable Energy Reviews 2015, 43, 1182-1198.

6 Syam Sundar L, Hashim Farooky Md, Naga Sarada S, Singh M K, Experimental thermal conductivity of ethylene glycol and water mixture based low volume concentration of Al_2O_3 and CuO nanofluids, Int Communications in Heat and Mass Transfer 2013;41:41-46;

7 Yiamsawasd T, Dalkilic A S, Wongwises S, Measurement of thermal conductivity of titania and alumina nanofluids, Thermochimica Acta 2012;545:48-56;

8 Minsta H A, Roy G, Nguyen C T, Doucet D, New temperature dependent thermal conductivity data for water-based nanofluids, Int J Therm Sci 2009;48:363–371;

9 Colangelo G, Favale E, de Risi A, Laforgia D, Results of experimental investigations on the heat conductivity of nanofluids based on diathermic oil for high temperature applications, Appl Energy 2012; 97:828–833;

10 Yurong H, Yi J, Haisheng C, Yulong D, Daqiang C, Huilin L, Heat transfer and flow behavior of aqueous of TiO_2 nanoparticles (nanofluids) flowing through a vertical pipe, Int J Heat Mass Transfer 2007;50:2272–2281;

11 Nnanna A, Experimental model of temperature-driven nanofluids, J Heat Transfer 2007;129:697–704;

12 Heyhat M M, Kowsary F, Rashidi A M, Esfehani S A V, Amrollahi A, Experimental investigation of turbulent flow and convective heat transfer characteristics of alumina water nanofluids in fully developed flow regime, International Communication in Heat and Mass Transfer 2012;39:1272-1278;

13 Hwang K S, Jang S P, Choi S U S, Flow and convective heat transfer characteristics of water-based Al_2O_3 nanofluids in fully developed laminar flow regime, Int J Heat Mass Transfer 2009;52:193–199;

14 Kim D, Kwon Y, Cho Y, Li C, Cheong S, Hwang Y, Convective heat transfer characteristics of nanofluids under laminar and turbulent flow conditions, Curr Appl Phys 2009;9:119–123;

15 Fotukian S M, Esfahany M N, Experimental study of turbulent convective heat transfer and pressure drop of dilute CuO/water nanofluid inside a circular tube, International Communications in Heat and Mass Transfer 2010;37:214–219;

16 Wen D, Ding Y, Experimental investigation into convective heat transfer of nanofluids at the entrance region under laminar flow conditions, International Journal of Heat and Mass Transfer 2004;47:5181–188;

17 Zeinali Heris S, Nasr Esfahany M, Etemad S Gh, Experimental investigation of convective heat transfer of Al_2O_3/water nanofluid in circular tube, Int J of Heat and Fluid Flow 2007;28:203–210;

18 Heris S Z, Etemad S G, M N Esfahany, Experimental investigation of oxide nanofluids laminar flow convective heat transfer, International Communications in Heat and Mass Transfer 2006; 33 : 529–535;

19 Anoop K B, Sundararajan T, Das S K, Effect of particle size on the convective heat transfer in nanofluid in the developing region, Int J of Heat and Mass Transfer 2009;52:2189–195;

20 Sahin B, Gültekin G G, Manay E, Karagoz S, Experimental investigation of heat transfer and pressure drop characteristics of Al_2O_3–water nanofluid, Experimental Thermal and Fluid Science 2013;50:21–28;

21 Taylor R A, Phelan PE, Otanicar T P, Tyagi H. Trimble, S., 2010. Applicability of nanofluids in concentrated solar energy harvesting, Proceedings of the ASME 2010, 4th International Conference on Energy Sustainability;1: 825-832;

22 Otanicar T P, Phelan P E, Prasher R S, Rosengarten G, Taylor R A, Nanofluid-based direct absorption solar collect, Journal of Renewable and Sustainable energy 2010;2(3);

23 Yousefi T, Veysi F, Shojaeizadeh E, Zinadini S, An experimental investigation on the effect of Al_2O_3-H_2O nanofluid on the efficiency of flat-plate solar collector, Renewable Energy 2012;39:293-298;

24 Chaji H, Ajabshirchi Y, Esmaeilzadeh E, Zeinali Heris S, Hedayatizadeh M, Kahani M, Experimental Study on Thermal Efficiency of Flat Plate Solar Collector Using TiO_2/Water Nanofluid, Modern Applied Science 2013;7:60-69;

25 Moghadam A. J., Farzane-Gord M., Sajadi M., Hoseyn-Zadeh M., Effects of CuO/water nanofluid on the efficiency of a flat plate solar collector, Exp. Therm. Fluid Sci. 58 (2014) 9-14;

26 Colangelo G, Favale E, De Risi A, Laforgia D, A new solution for reduced sedimentation flat panel solar thermal collector using nanofluids, Applied Energy 2013;111:80-93;

27 EN 12975-2;

28 Fisher S, Heidemann W, Steinhagen H M, Perers B, Bergquist P, Hellström B, Collector test method under quasi-dynamic conditions according to the European Standard EN 12975-2, Solar Energy 2004;76:117-123;

29 Keblinski P, Phillpot SR, Choi SUS, Eastmam LA. Mechanisms of heat flow in suspensions of nano-sized particles (nanofluids). Int J Heat Mass Transfer2000;45:855–63;

30 Jang SP, Choi SUS. Effects of various parameters on nanofluids thermal conductivity. J Heat Transfer 2007;129(May):617–23.

31 Xuan Y, Li Q, Investigation in convective heat transfer and flow features of nanofluids, J Heat Transfer 2003;125(February):151–155.

Figure Captions

Figure 1 – Delta backscattering measurement of Al_2O_3 water based nanofluid at 3 %vol

Figure 2 – Cluster dimension of Al_2O_3 water based nanofluid at 3 %vol

Figure 3 – Tubes and copper plate fixed and coated with black paint (Absorber)

Figure 4– Flat panel solar thermal collector

Figure 5– Flow in a traditional flat panel solar thermal collector

Figure 6– Top header (or bottom header) with modified internal shaped element

Figure 7-Layout of experimental setup

Figure 8– a) Experimental setup and b) flat panel solar thermal collector

Figure 9– Thermal efficiency of solar collector with water (mass flow rate 0.02±0.0008 kg/s) and Al_2O_3 – bi-distillated water 3.0 %vol (mass flow rate 0.02±0.0015 kg/s)

Table Captions

Table 1 – Test conditions and deviation

Table 2 – Measurement uncertainties

Table 3– Experimental results for bi-distillated water

Table 4– Experimental results for Al_2O_3 – bi-distillated water nanofluid 3.0 %vol

Table 5 - Values of the zero loss collector efficiency η_0, the heat transfer coefficient a_1 and the uncertainty coefficient R^2

Figure 1

Click here to download high resolution image

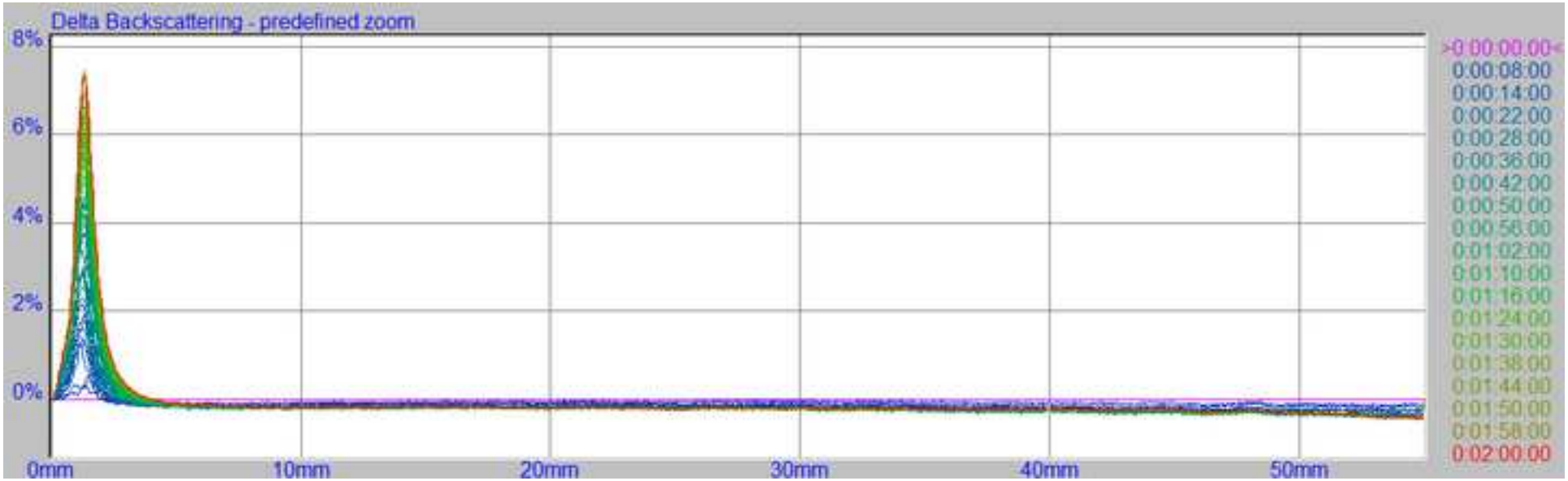

Figure 2

Click here to download high resolution image

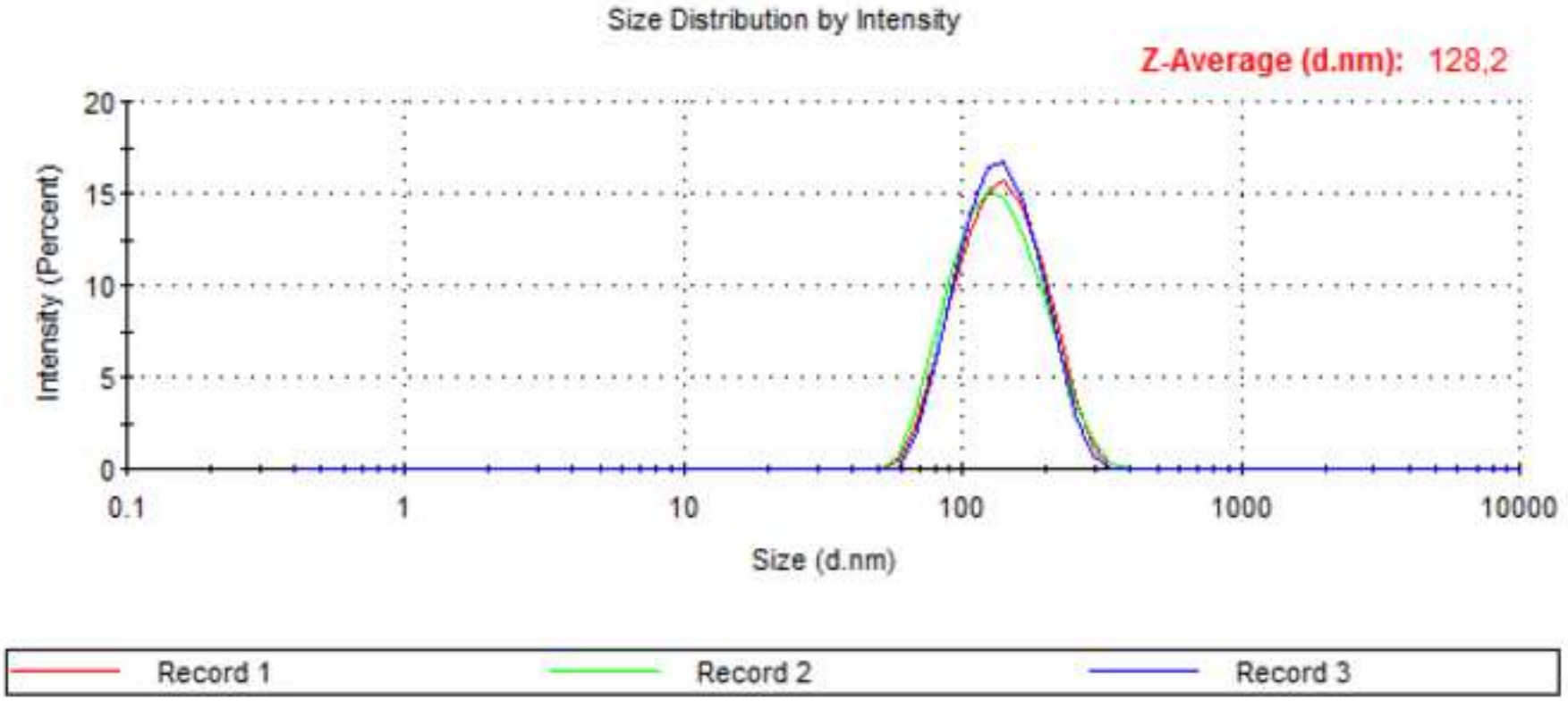

Figure 3

Click here to download high resolution image

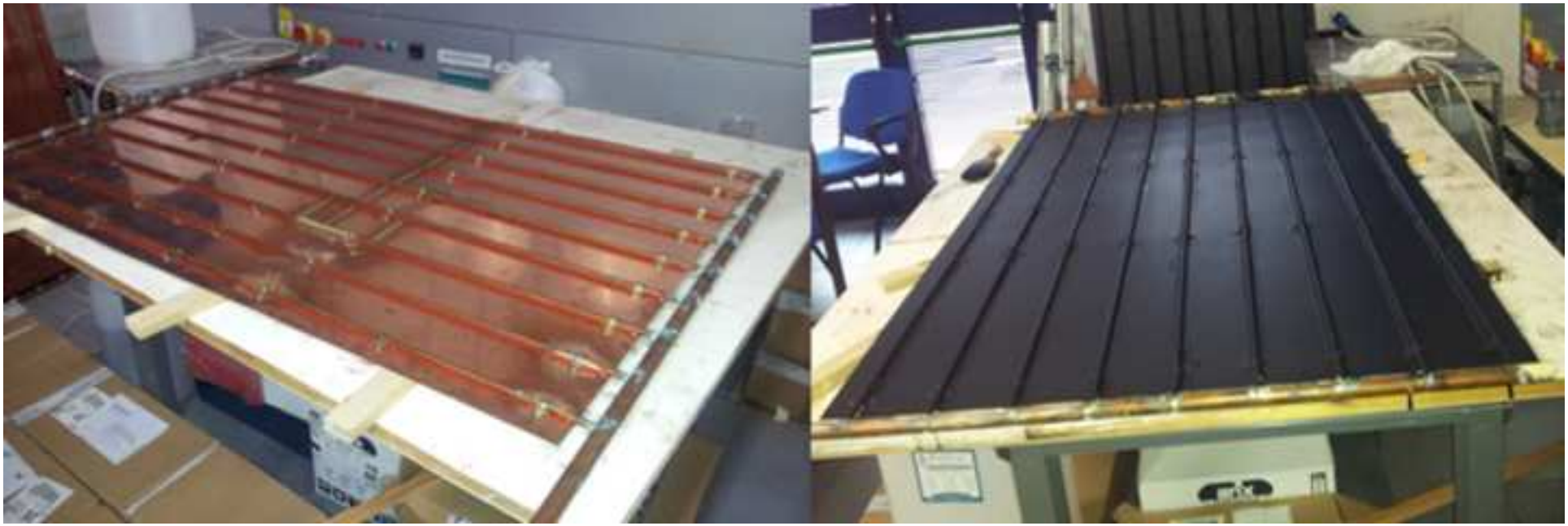

Figure 4

Click here to download high resolution image

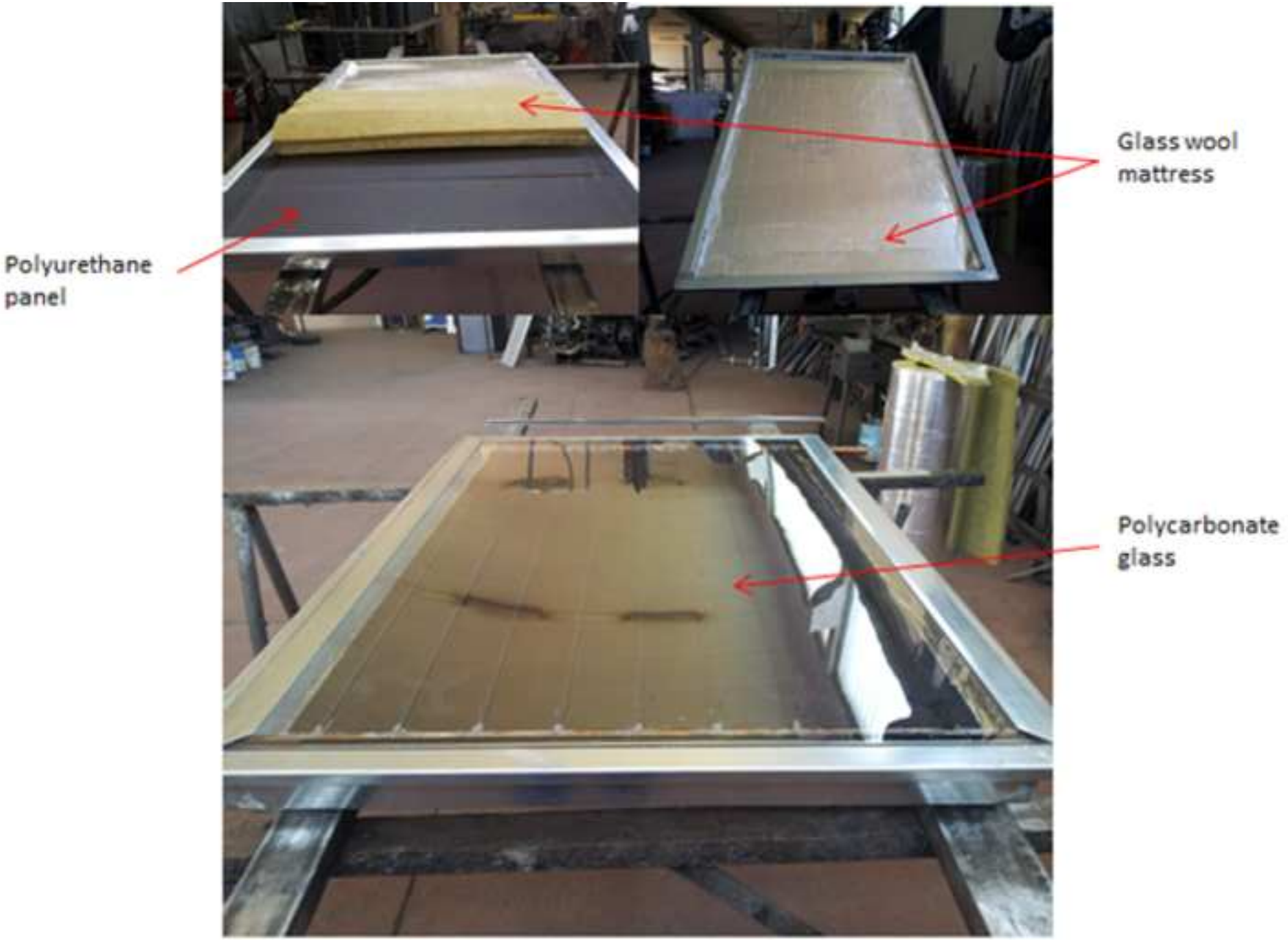

Figure 5

Click here to download high resolution image

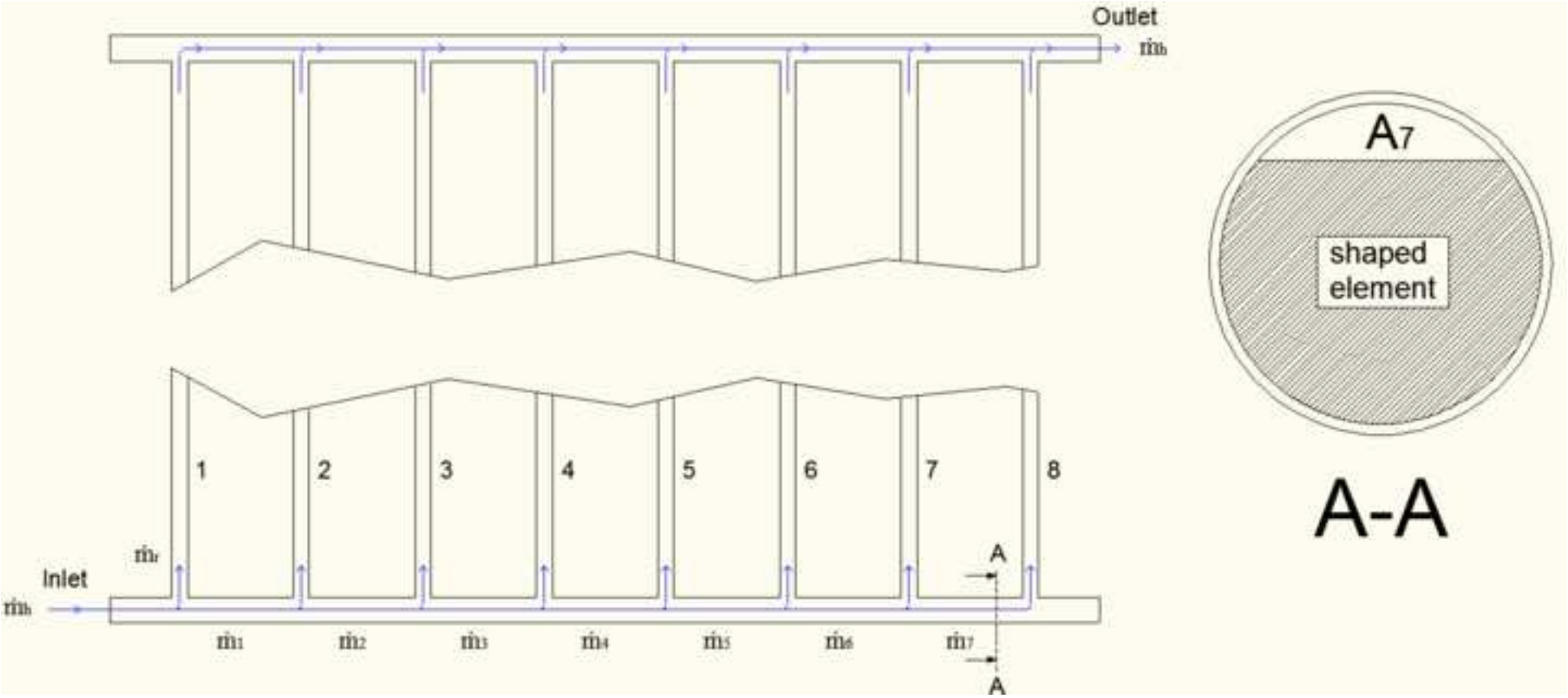

Figure 6

Click here to download high resolution image

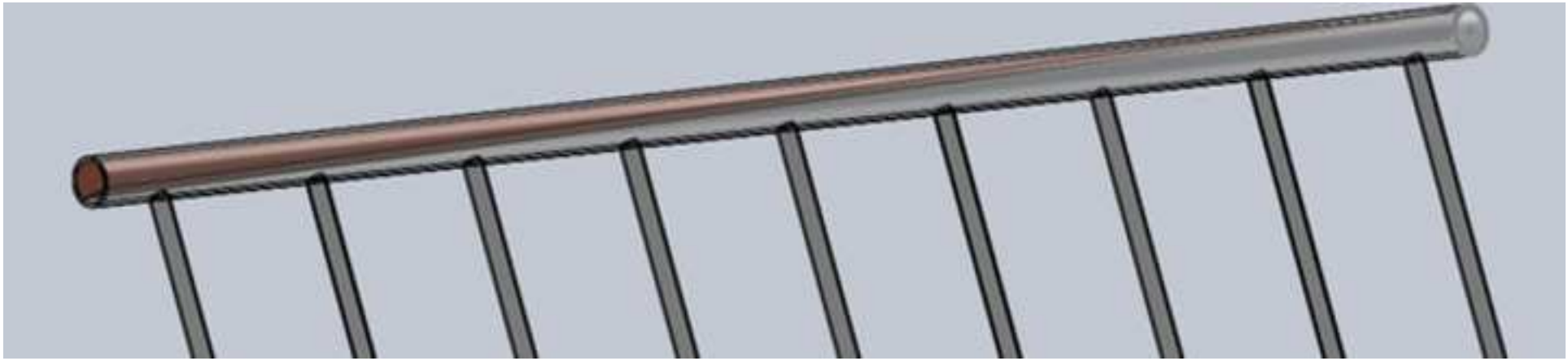

Figure 7
Click here to download high resolution image

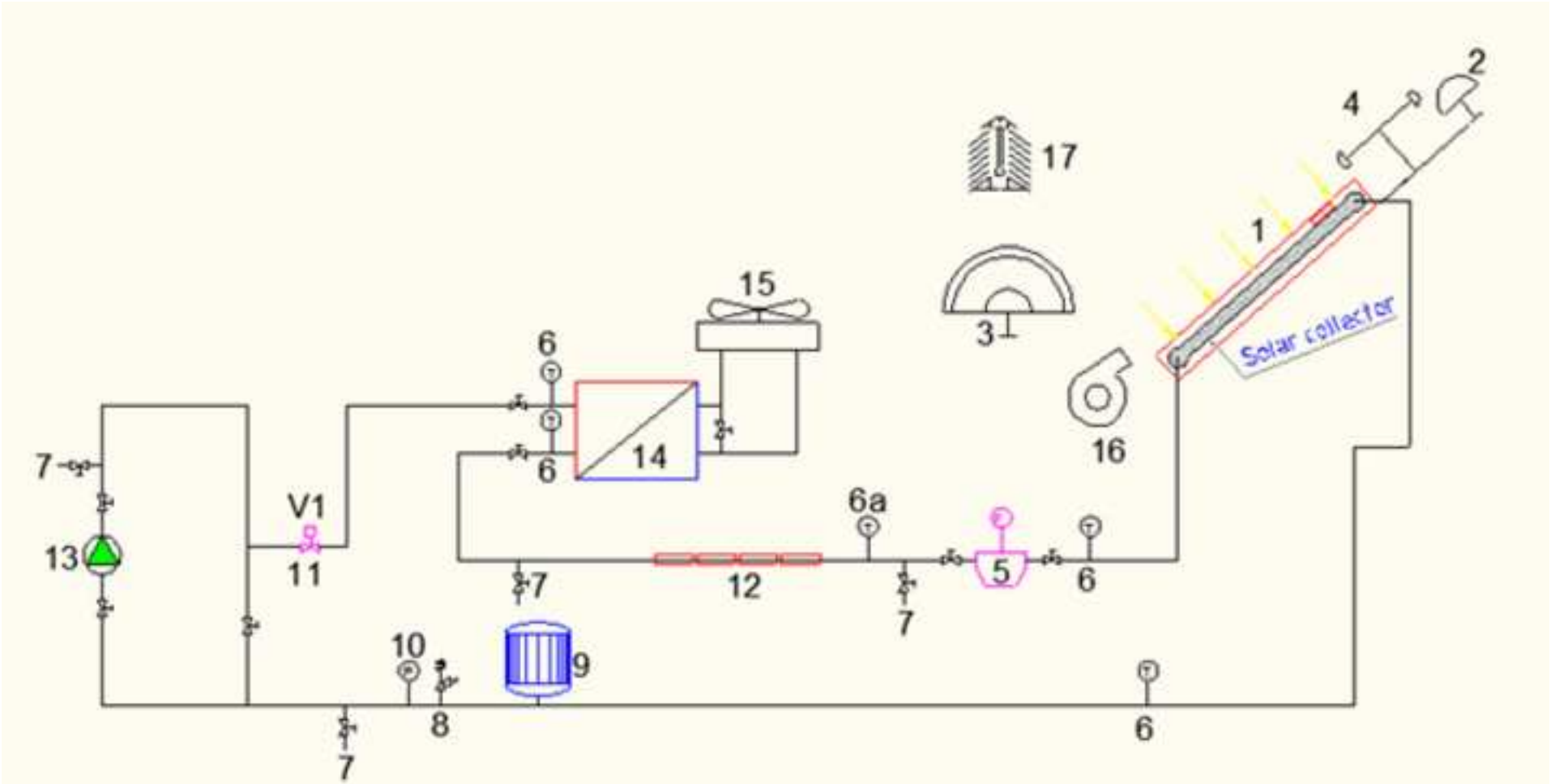

Figure 8
Click here to download high resolution image

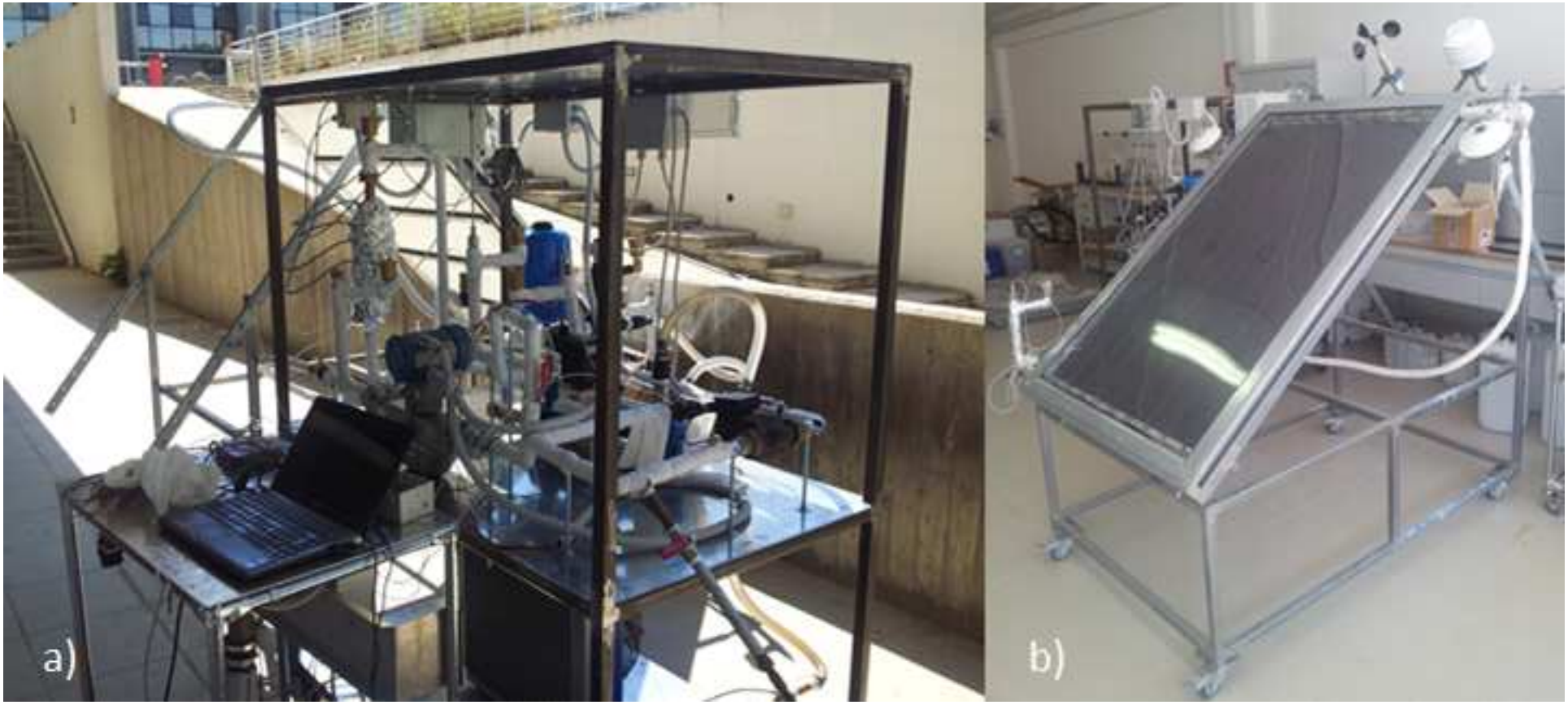

Figure 9

Click here to download high resolution image

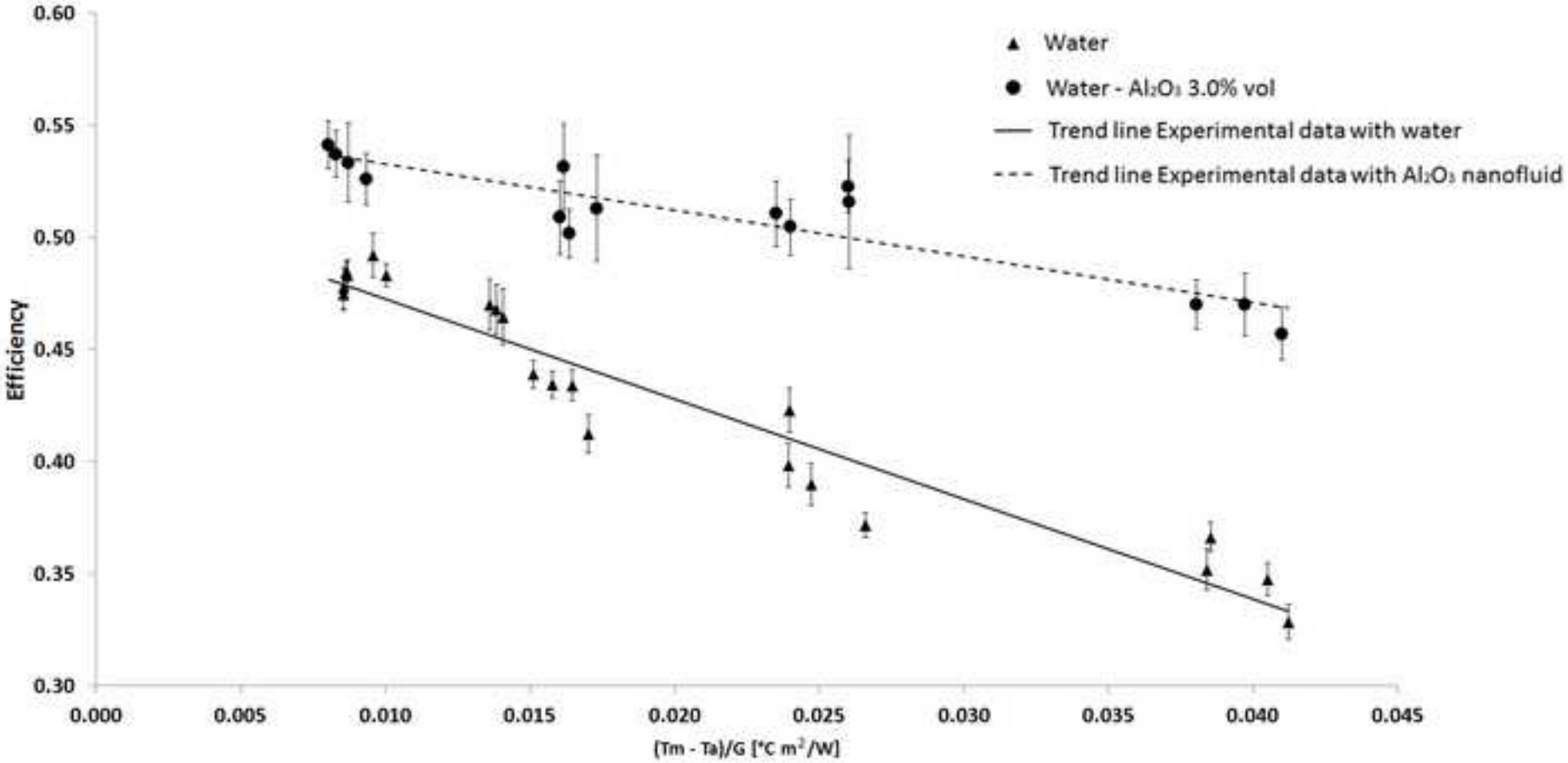

Table 1 – Test conditions and deviation

Parameter	Value	Deviation
Global solar irradiance G [W/m^2]	>700	±50
Incidence angle of beam irradiance θ [°]	<20	-
Surrounding air temperature t_a [°C]	-	±1
Diffuse fraction G_d/G [%]	<30	-
Surrounding air speed u [m/s]	3	±1
Collector inlet temperature t_{in} [°C]	-	±0.1

Table 2 – Measurement uncertainties

	Uncertainty
Mass flow rate $\dot{m}$	<1.0%
Outlet temperature T_{out}	<0.1 °C
Inlet temperature T_{in}	<0.1 °C
Solar radiation G	<2.0%

Table 3

Table 3 – Experimental results for bi-distillated water

Test number	T^*_m[°C m^2/W]	T_a [°C]	G [W/m^2]	$\dot{m}$[kg/s]	T_{out} [°C]	T_{in} [°C]	η	U_η (%)
1	**0.00855**	32.11	916.49	0.020231	42.82	37.07	**0.4747**	0.69
2	**0.00855**	32.30	899.79	0.020162	42.84	37.14	**0.4775**	0.60
3	**0.00866**	22.87	972.21	0.020921	34.30	28.27	**0.4847**	0.71
4	**0.00869**	23.12	963.17	0.020986	34.46	28.52	**0.4834**	0.76
5	**0.00958**	24.34	987.63	0.020408	36.99	30.62	**0.4921**	1.49
6	**0.01004**	22.62	942.69	0.020791	35.02	29.16	**0.4832**	0.89
7	**0.01359**	24.20	973.14	0.019727	40.55	34.31	**0.4700**	0.62
8	**0.01384**	24.78	980.84	0.019674	41.47	35.23	**0.4679**	0.77
9	**0.01406**	25.27	956.42	0.020185	41.68	35.75	**0.4646**	0.76
10	**0.01512**	34.29	820.82	0.019447	49.17	44.21	**0.4389**	1.05
11	**0.01576**	34.11	801.80	0.019145	49.18	44.31	**0.4346**	1.04
12	**0.01646**	33.65	846.06	0.019662	50.07	45.07	**0.4340**	0.94
13	**0.01702**	33.17	889.95	0.019990	50.63	45.72	**0.4123**	1.07
14	**0.02393**	22.35	943.73	0.020203	47.42	42.44	**0.3984**	1.23
15	**0.02396**	24.56	941.32	0.021162	49.62	44.59	**0.4229**	1.42
16	**0.02471**	22.26	914.83	0.020125	47.24	42.49	**0.3899**	1.05
17	**0.02659**	33.44	867.68	0.019960	58.67	54.34	**0.3718**	1.01
18	**0.03839**	33.76	879.95	0.019960	69.62	65.47	**0.3520**	2.41
19	**0.03852**	33.53	896.66	0.019344	70.33	65.79	**0.3663**	1.47
20	**0.04051**	33.43	864.14	0.019645	70.44	66.41	**0.3475**	1.74
21	**0.04121**	33.59	840.78	0.019592	70.12	66.35	**0.3285**	2.04

Table 4

Table 4 – Experimental results for Al_2O_3 – bi-distillated water nanofluid 3.0 % vol

Test number	T*m[°C m^2/W]	Ta [°C]	G [W/m^2]	ṁ[kg/s]	Tout [°C]	Tin [°C]	η	Uη (%)
1	**0.00804**	33.37	849.06	0.020342	43.29	37.09	**0.5412**	0.91
2	**0.00829**	33.08	895.36	0.021403	43.58	37.42	**0.5372**	1.03
3	**0.00871**	25.61	919.29	0.019972	36.86	30.36	**0.5153**	3.30
4	**0.00934**	25.43	917.48	0.020061	37.29	30.69	**0.5260**	2.20
5	**0.01604**	35.54	873.83	0.021350	52.41	46.70	**0.5089**	1.10
6	**0.01616**	28.79	921.98	0.019736	46.86	40.05	**0.5314**	2.85
7	**0.01636**	33.68	895.45	0.021614	51.18	45.48	**0.5018**	0.79
8	**0.01731**	33.59	847.80	0.021028	51.10	45.43	**0.5130**	2.24
9	**0.02351**	33.11	917.59	0.022700	57.51	51.85	**0.5106**	2.12
10	**0.02401**	32.74	912.74	0.020898	57.60	51.70	**0.5046**	1.20
11	**0.02601**	34.77	895.39	0.021015	61.11	55.01	**0.5227**	0.72
12	**0.02604**	29.72	944.86	0.020847	57.53	51.12	**0.5159**	1.56
13	**0.03805**	32.59	896.30	0.019328	69.67	63.70	**0.4700**	1.94
14	**0.03971**	32.45	868.34	0.019772	69.76	64.10	**0.4699**	2.61
15	**0.04099**	32.60	839.88	0.019650	69.67	64.31	**0.4570**	2.12

Table 5 - Values of the zero loss collector efficiency η_0, the heat transfer coefficient a_1 and the uncertainty coefficient R^2

Working Fluid	η_0	a_1 [W/m^2 °C]	R^2
Water	0.517	4.452	0.925
Al_2O_3 - water nanofluid 3.0 %vol	0.553	2.053	0.819